

Development of a Low-Cost Parallel Kinematic Machine for Multidirectional Additive Manufacturing

Xuan Song

Daniel J. Epstein Department of Industrial and Systems Engineering,
University of Southern California,
Los Angeles, CA 90089

Yayue Pan

Department of Mechanical and Industrial Engineering,
University of Illinois at Chicago,
Chicago, IL 60607

Yong Chen¹

Daniel J. Epstein Department of Industrial and Systems Engineering,
University of Southern California,
Los Angeles, CA 90089
e-mail: yongchen@usc.edu

Most additive manufacturing (AM) processes are layer-based with three linear motions in the X, Y, and Z axes. However, there are drawbacks associated with such limited motions, e.g., nonconformal material properties, stair-stepping effect, and limitations on building-around-inserts. Such drawbacks will limit AM to be used in more general applications. To enable 6-axis motions between a tool and a work piece, we investigated a Stewart mechanism and the feasibility of developing a low-cost 3D printer for the multidirectional fused deposition modeling (FDM) process. The technical challenges in developing such an AM system are discussed including the hardware design, motion planning and modeling, platform constraint checking, tool motion simulation, and platform calibration. Several test cases are performed to illustrate the capability of the developed multidirectional AM system. A discussion of future development on multidirectional AM systems is also given. [DOI: 10.1115/1.4028897]

Keywords: additive manufacturing, multidirection, parallel kinematic machine, fused deposition modeling, building-around-inserts

1 Introduction

AM processes can directly fabricate three-dimensional (3D) computer-aided design (CAD) models by controlling the selective accumulation of materials. Most AM processes are layer-based, that is, a given 3D model is first sliced into a set of two-dimensional (2D) layers; accordingly, a physical part is fabricated by stacking the sliced 2D layers together to approximate the given CAD model. An example of a tilted rod (*AB*) using the layer-based AM processes is shown in Fig. 1. For such AM processes, only the linear motions in the X, Y, and Z axes are required.

The layer-based fabrication approach has many benefits. For example, (1) tool path planning and hardware design are simplified; and (2) complex shapes that are impossible to be made before can be fabricated. However, there are also drawbacks associated with the layer-based fabrication approach. For example, (1) the surface finish is poor due to the stair-stepping effect (refer to rod *AB* in Fig. 1); (2) the material property of a geometric feature will depend on the building direction used in the fabrication process. Consequently, the material property of a tilted rod in different tilting angles will be different. In addition, (3) it would be difficult to build parts around inserts (e.g., embedding electric or optical components) due to the limited tool motions that are allowed in the system.

To address the problems of the layer-based AM processes, various methods have been proposed. For example, controlled cure depth [1,2], postprocessing [3,4] and meniscus methods [5,6] have been developed for improving surface finish; and techniques such as model shape modification [7] and hybrid process development [8] have been employed to enhance the fabrication capability of building-around-inserts. However, most approaches can only improve one or a few drawbacks in a limited fashion mainly due to the use of a single build direction (Z axis) and a uniform layer

thickness in the building process. In comparison, multidirectional AM processes, in which materials are added along multiple directions using nonuniform layer thickness, can address many limitations of the layer-based AM processes. We believe both layer-based and nonlayer-based material deposition approaches will be employed in future AM processes.

To achieve multi-axis motions between accumulative tools and a workpiece, multidirectional AM processes can be classified into (1) platform based and (2) accumulative tool based approaches.

(1) Platform based approaches. Multidirectional fabrication can be achieved by rotating the platform in order to orientate the workpiece related to the accumulative tool. For example, a customized compliant parallel kinematic machine is presented in Ref. [9] for the multidirection layered deposition process. The machine is comprised of two parts: an *X-Y* overhang head unit, and a workpiece orientation unit to rotate the built part to have a building direction that is aligned to the head unit. Consequently, the deposition head can add materials from different orientations. The laser direct casting process [10] uses a similar approach by rotating built parts to achieve multidirectional fabrication. A multidirectional UV lithography process at micro- and nanoscales is discussed in Ref. [11], in which two step motors are used to control the tilting and rotational angles of the substrate. In the design of a laser direct metal deposition (DMD) system [12] for repairing deep and internal cracks in metallic components, the laser beam is kept stationary while the workpiece is moved and rotated.

(2) Accumulative tool based approaches. In multidirectional AM processes, the accumulative tools, instead of the platform, can be oriented with multiple degrees of freedom. A multidirectional DMD system using a high-power laser is presented in Refs. [13–16]. The laser beam is focused onto a workpiece and produces a melting pool. Metal powders are injected into the melting pool by feeding with inert gas stream. In the system, the laser head is controlled by a 5-axis motion mechanism that allows deposition of given shapes. As shown in Ref. [16], the slicing direction can be

¹Corresponding author.

Contributed by the Manufacturing Engineering Division of ASME for publication in the JOURNAL OF MANUFACTURING SCIENCE AND ENGINEERING. Manuscript received April 15, 2014; final manuscript received October 14, 2014; published online December 12, 2014. Assoc. Editor: David L. Bourell.

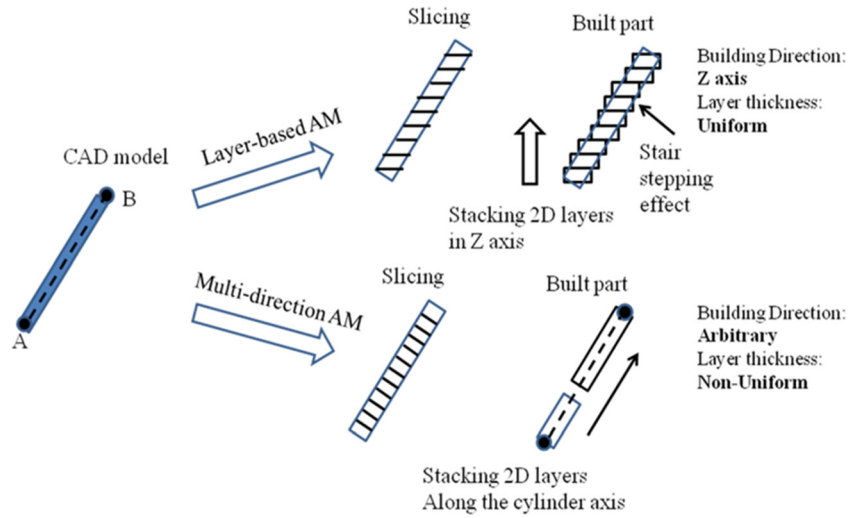


Fig. 1 A schematic illustration of layer-based and multidirectional AM processes

arbitrary, and a number of layers with nonuniform thicknesses can be generated. Accordingly, the tool path planning software can convert CAD models into nozzle motions for multi-axis deposition. The directed light fabrication process [17] is another kind of DMD process that fuses inert-gas-delivered metal powders into the focal zone of a high powered laser beam. By using the multi-axis numerical control sequence tool paths, materials can also be deposited in varying orientations. For the fabrication of polymer-based objects, a computer numerically controlled accumulation process was developed [18], in which a fiber optical cable connected with a UV-LED (Light Emitting Diode) is controlled by a 5-axis motion system to enable the X , Y , and Z axes translations and the A and B axes rotations. Therefore, the accumulative tool can cure liquid resin in various directions.

Compared with the tool based approaches, the platform based processes have simpler structures. However, rotating an accumulative tool instead of the platform is more flexible in achieving desired relative motions. In the past few years, various low-cost 3D printers (e.g., MakerBot, Solidoodle, Cube, Robox, etc.) using the X , Y , and Z linear motions have been developed with a price around \$500–\$2000. Some nontraditional designs to achieve the linear motions have also been developed (e.g., RepRap Mini Kossel based on a delta design, refer to Fig. 2). However, at the moment, it is not clear whether a low-cost multidirectional 3D printer is feasible; and if so, what should be its design?

To enable 6-axis motions between a tool and a work piece, a Stewart mechanism is investigated in this paper for developing a low-cost multidirectional 3D printing system. An FDM heating extruder is considered as the accumulative tool in our study. Compared with the traditional translation and rotation based approach, the Stewart mechanism enables the AM system to be less bulky.

The rest of the paper is organized as follows. Section 2 introduces the hardware design based on the Stewart mechanism. The cost of the prototype system is also discussed. In Sec. 3, a kinematic modeling and simulation software system is presented. A laser-camera system is also discussed to reduce the deposition gap errors. Section 4 describes a calibration method to achieve improved accuracy of the parallel kinematic machine. Section 5 presents the data processing pipeline of the multidirectional AM system based on the machine. Section 6 demonstrates the fabrication process of the prototype multidirectional FDM system with a discussion of the experimental results. Finally, conclusions are drawn in Sec. 7.

2 Hardware Design

There exist many different ways of achieving multi-axis motion of the extruder. Figure 3 shows two 6-axis robotic arms of both industrial and desktop levels. The industrial robotic arm is extremely expensive for our application, although it is relatively accurate and rigid. The desktop level robotic arm is quite affordable, but its low rigidity and accuracy cannot meet the requirement of AM. An alternative way is to integrate multiple rotations with the XYZ translations. However, as demonstrated in our previous work [18], the machine is bulky and the process is relatively slow. The recent development of 3D printers based on the Delta design (e.g., Orion Delta from SeeMeCNC and Mini Kossel from RepRap) demonstrate that the Delta design can achieve much faster linear motions than the traditional design based on the X , Y , and Z linear stages. It motivates us to investigate similar designs for multidirectional AM processes.

To enable the 6DoF motion of a tool with respect to a fixed frame, six length-changeable struts are used to connect a moving platform on which an accumulative tool is mounted. For each strut, one of its ends is connected to the moving platform by a 3DoF joint, and another end is connected to a fixed base frame by a 2DoF joint (refer to Fig. 3(a)). This 6-axis parallel kinematic machine is also called Gough-Stewart mechanism. The mechanism has been used in precision positioning system (e.g., Hexapod 6-axis parallel positioning systems from Physik Instrumente). However, the commercial systems are expensive (>\$20 K) with relatively small travel ranges (<50 mm). They are not suitable for developing a low-cost multidirectional 3D printing system.

Motivated by the recent progress on developing low-cost 3D printers using the Delta design, we investigate the feasibility of using low-cost components in developing a 6-axis parallel positioning system with sufficient accuracy for AM processes. It is shown, with the aid of an integrated position sensor and related tool path planning software systems (refer to Sec. 3), a

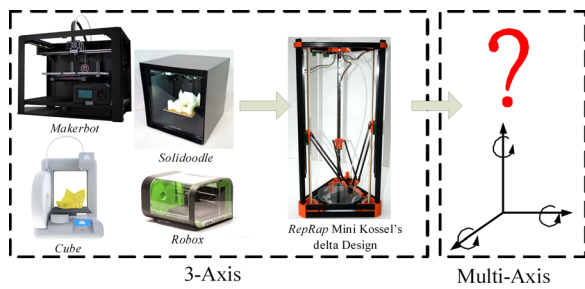


Fig. 2 Some low-cost 3D printers on market for the layer-based material deposition

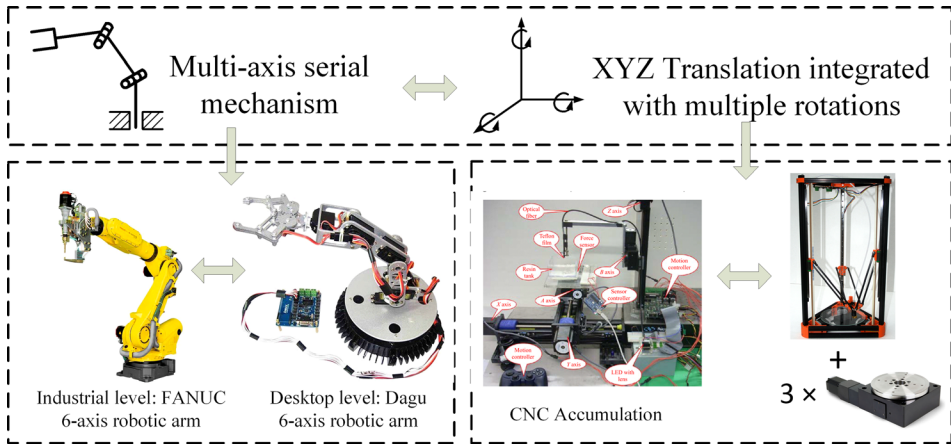


Fig. 3 Alternative mechanisms to achieve multi-axis extrusion

multidirectional 3D printer with a price around \$2500 is feasible. The hardware components of our parallel kinematic machine are introduced as follows.

As shown in Fig. 4(a), the parallel kinematic machine is made up of six length-changeable struts. In our testbed, six ball screw linear actuators are used for the purpose. The linear actuators are connected in pairs to a hexagon moving platform by ball joints. Each motor body is mounted on a customized universal joint, which has 2DoF motion relative to the fixed base frame. The CAD model of the designed system is shown in Fig. 4(b). Linear actuators from Eastern Air Devices Inc. (Dover, NH) are used in our testbed. Its original lead-screw was replaced by a 1/4–16 ACME one with a length of 12 in. The system is controlled by a high performance 8-axis motion control board KFLOP + 2KSTEP (Dynomotion Inc., Calabasas, CA). A motion parameter generation and control software system has been developed. The system can load in the G-code of tool paths, transform them into motion command parameters, and send them to the motion controller through six output pins in the KSTEP board. A photo of the built prototype system is shown in Fig. 13. Based on the Stewart mechanism, relatively small motions of the linear actuators can lead to large motions of the tool on the moving platform. Consequently, the multidirectional AM system can have high fabrication speed.

The detail design of a length-changeable strut based on a non-captive linear motor is also shown in Fig. 4(b). For the linear actuator, it creates linear motions only when the end of the lead screw has a holding torque. To impose the required torque, we use a pair of slide bushings with two guide rails on each motor. Our design has good modularity since all the struts in the designed system are exactly the same.

Due to its motion in six degrees of freedom, the Stewart platform has been studied for the 5-axis machining before (e.g., Refs. [19] and [20]). However, the Stewart platform has not been widely used in the multi-axis CNC machining. One of the main reasons is the rigidity of the Stewart platform is not sufficient for the cutting process. Hence, the machining accuracy would be poor. Compared to the cutting force in the machining process, the typical forces in AM processes are relatively small. For example, during the operation of the FDM process, the main loads are the friction from extruding melted filament against the platform. This low-load working condition enables much simpler hardware design such as joints. Furthermore, different from the CNC machining processes, the rigidity of the Stewart platform may be sufficient for the AM processes, which is investigated in the paper.

In our prototype system, a 0.4 mm nozzle extruder is used. Accordingly, the minimum motion resolution of the extruder is 0.4 mm. To ensure the building process to be successful, the deposition gap between the nozzle tip and the building platform or previously built layers should be less than 0.2 mm. In this paper, an error compensation method based on a laser-camera position sensor is developed. The integrated laser-camera position sensor can ensure the developed Stewart platform to have a deposition gap to be precisely at 0.1 mm. The extrusion material used in our study is acrylonitrile butadiene styrene (ABS), whose working temperature is between 200 °C–250 °C.

The total cost of the main hardware components used in our prototype system is less than \$1500 excluding the base frame (refer to Table 1 in Appendix A for a list of the components and the related cost). Compared to commercial hexapod machines, the prototype

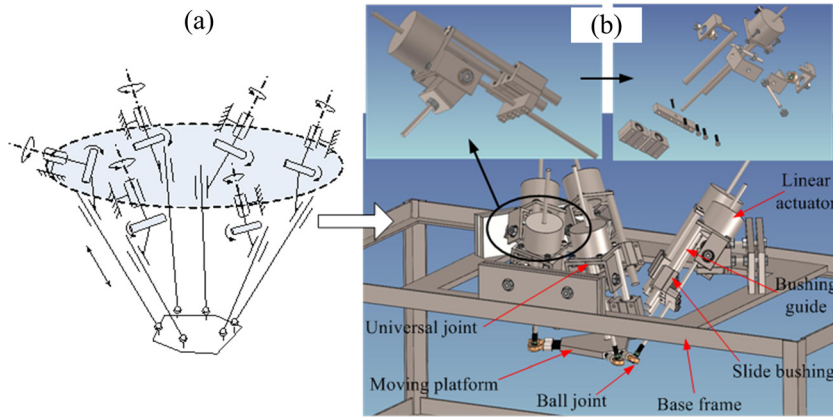


Fig. 4 A schematic illustration of a Stewart mechanism and the CAD design of our parallel kinematic machine

system has a much lower cost, which is critical for developing low-cost multidirectional 3D printers in the future. The Stewart-mechanism-based system is general. It allows accumulative tools with any 6-axis motions using various material deposition principles. In the paper, the FDM process is demonstrated using the developed prototype system. Other AM processes can also be used by mounting different accumulative tools on the platform. In addition, the system has low inertia with small energy consumption, since all the motions are conducted by moving accumulative tools, which are generally lighter than the workpiece.

3 Motion Planning and Software System Design

The desired tool motion in the 6-axis parallel kinematic machine needs to be converted into the linear motions of the six

length-changeable struts. Accordingly, the motion controller can be used to control the linear actuators to move required displacements and rotations.

3.1 System Coordinate Transformation. In the motion planning, quaternion \mathbf{q} is used in describing the pose of the moving platform. That is, for a rotation angle θ around a unit vector $(v_x, v_y, v_z)^T$, its quaternion \mathbf{q} is described as

$$\begin{aligned}\mathbf{q} &= (q_1, q_2, q_3, q_4)^T \\ &= \left(\cos\left(\frac{\theta}{2}\right), v_x \sin\left(\frac{\theta}{2}\right), v_y \sin\left(\frac{\theta}{2}\right), v_z \sin\left(\frac{\theta}{2}\right) \right)^T\end{aligned}\quad (1)$$

Accordingly, the rotation matrix can be obtained using quaternion elements

$$\mathbf{R}(\mathbf{q}) = \begin{pmatrix} q_1^2 + q_2^2 - q_3^2 - q_4^2 & 2q_2q_3 - 2q_1q_4 & 2q_2q_4 + 2q_1q_3 \\ 2q_2q_3 + 2q_1q_4 & q_1^2 - q_2^2 + q_3^2 - q_4^2 & 2q_3q_4 - 2q_1q_2 \\ 2q_2q_4 - 2q_1q_3 & 2q_3q_4 + 2q_1q_2 & q_1^2 - q_2^2 - q_3^2 + q_4^2 \end{pmatrix} \quad (2)$$

To establish the transformation model from the given quaternion to the absolute displacement of the six axes, two coordinate systems are shown in Fig. 5(a). One coordinate system is attached to the fixed base frame (B) and another one is fixed on the moving frame (P). Initially, the moving frame has the same coordinate axes as those of the base frame (refer to O_P and O_B in Fig. 5(a)). During the fabrication process, the coordinate system of the moving frame is aligned with the accumulation tool and will be different from the original one.

Suppose any platform pose is given as $(x_{op}, y_{op}, z_{op}, \mathbf{q})$. Its first part, (x_{op}, y_{op}, z_{op}) is the origin position of the moving frame. The second part, \mathbf{q} , is the quaternion of the moving frame after the rotation from its initial position. Both of them are defined in terms of the coordinate system of the base frame. Accordingly, we know

$$\overrightarrow{P_i B_i}^B = \overrightarrow{O_B B_i}^B - \overrightarrow{O_B O_P}^B - \mathbf{R} \cdot \overrightarrow{O_P P_i}^P \quad (3)$$

where $\overrightarrow{P_i B_i}^B$ is the vector $\overrightarrow{P_i B_i}$ defined in the coordinate system of the base frame B ; $\overrightarrow{O_B B_i}^B$ is the position of the universal joint B_i in terms of the coordinate system of the base frame; $\overrightarrow{O_B O_P}^B$ is the position of the tool tip; $\overrightarrow{O_B O_P}^B = (x_{op}, y_{op}, z_{op})$; $\overrightarrow{O_P P_i}^P$ is the position of the ball joint in the moving frame; \mathbf{R} is the rotation matrix that is calculated by Eq. (2); and $i = 0, 1, \dots, 5$. Consequently, the displacement Δl_i of the i th strut is

$$\Delta l_i = \left\| \overrightarrow{P_i B_i}^B \right\| - l_{i0}$$

where l_{i0} is the initial joint offset.

In our hardware design, the base joints are not exactly located on the legs (refer to Fig. 5(b)). Consequently, the deviation of the lead screw from the base joint needs to be considered when computing the displacement. That is

$$\Delta l_i = \sqrt{\left\| \overrightarrow{P_i B_i}^B \right\|^2 - \text{dev}^2} - l_{i0} \quad (4)$$

3.2 Tool Path Planning. As mentioned in Sec. 1, multidirectional AM could improve surface finish, optimize the direction of material deposition, and overcome the limitations in

building-around-inserts. In order to achieve these benefits, proper tool paths need to be planned. The 6-axis tool motions enabled in our prototype system provide tremendously large design freedom in planning the tool paths for desired performances. For example, in order to achieve improved surface finish of a curved surface as shown in Fig. 6(a), a possible tool path is to first offset the surface inside by a distance $n \cdot \delta$ (δ is the layer thickness and n is an offset layer number). A 3D offsetting algorithm can be used in computing the offset CAD model [21]. The computed offset CAD model can then be sliced into layers based on a given building direction. The sliced layers can be fabricated using the layer-based process, during which the tool orientation is kept vertical. Finally, the deposition tool moves along the curved surface with the tool orientation aligned with the surface normal during the building process. As shown in our experimental tests (refer to Sec. 6.1), the accordingly fabricated objects can achieve much better surface finish.

To build offset contours on an object surface or to build features around an inserted object, a tool path needs to be generated, e.g., starting at the point S and ending at point E (refer to Fig. 6(b)). Along the tool path, the tool keeps the same orientation as the current surface normal and moves along the tangent direction. Given any object, the nozzle tip will initially move to the start point S , and then extrudes materials along the planned tool path. Assume the tool pose at point S is $(x_s, y_s, z_s, \mathbf{q}_s)$. Except at the starting point S , any other point along the path is given as its relative movement $(\Delta x_i, \Delta y_i, \Delta z_i, \Delta \mathbf{q}_i)$ with respect to its previous point. Therefore, the tool pose at an intermediate point I is

$$\left(x_s + \sum_{i=S+1}^I \Delta x_i, y_s + \sum_{i=S+1}^I \Delta y_i, z_s + \sum_{i=S+1}^I \Delta z_i, \prod_{i=I}^{S+1} \Delta \mathbf{q}_i \cdot \mathbf{q}_s \right) \quad (5)$$

Then we can obtain control command for each strut using Eqs. (2)–(5). In Fig. 6, the solid circle denotes a sample position along the tool path, “T” represents the orientation of the tool, and the arrow is the moving direction of the tool.

3.3 Real-Time Feedback Control for Initial Deposition Gap. As discussed in Sec. 3.2, the accumulation tool starts at point S and then moves along the tool path to the end point E . The deposition gap at S is critical (< 0.2 mm); otherwise, the extruded materials will not be able to stick to the base surface. When it happens, the build will fail afterwards. Due to the low-cost

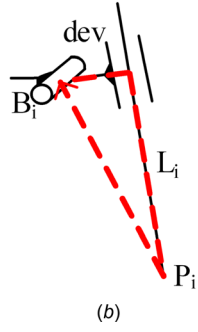
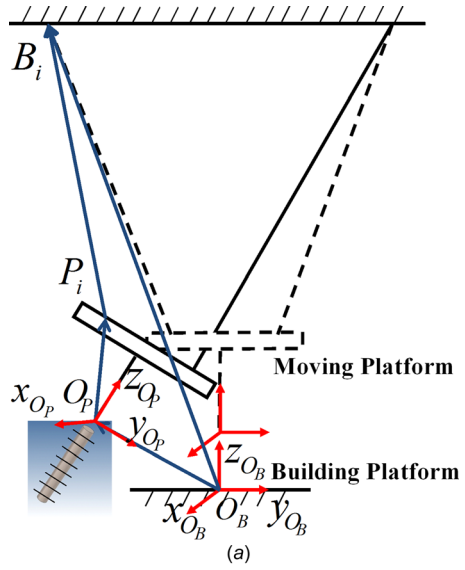


Fig. 5 An illustration of the coordinate systems and the main parameters of the prototyping system

components used in the prototype system and the building errors including the backlash in the joints, it was found that such a tight tolerance is difficult to achieve. That is, either the real gap between the nozzle tip and the base surface is larger than 0.2 mm, or the tip collides with the object. To address the problem, a low-cost online sensor using a laser and a camera is integrated in the prototype system. Accordingly, a control strategy for identifying the desired initial deposition gap is described as follows.

To avoid the undesired collision of the nozzle and the object at the starting point, the tool tip is first moved to a point S' . As shown in Fig. 7(a), S' is obtained by moving the desired starting point S outwards along the surface normal for a certain distance. Therefore, the final tool path use in our system is segment $S'S$ plus segment SE . Moving from S' toward the object, the tool will stop at point S , where the deposition gap distance is within the acceptance range. Then control commands for the six struts are dynamically generated and executed to move the tool along path SE to deposit materials. Since the translations and rotations from S' to S are known, and all the points along the tool path are given as relative displacements with respect to their previous points, this

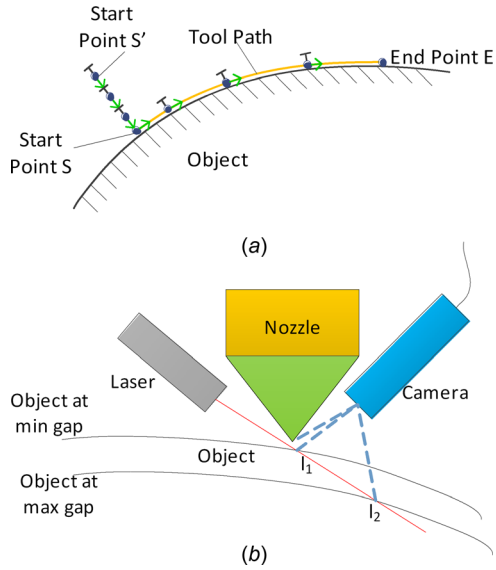


Fig. 7 An illustration of initial deposition gap control. (a) Adjusted starting point for tool path and (b) a laser-camera system to achieve initial deposition gap.

initial adjustment will not influence the following motion. In addition, the initial adjustment overcomes hardware errors such as the backlash in the joints. Hence, the desired gap between the tool tip and the base surface along path SE can be ensured.

In order to identify the desired deposition gap along $S'S$, a laser-camera system around the tool nozzle is integrated as shown in Fig. 7(b). A red laser (Laserglow Technologies, Toronto, Canada) is focused toward the nozzle tip, and its laser dot is captured by a microscope camera (Aven Inc., Ann Arbor) in real time. Since the position of the nozzle tip is fixed with respect to the camera, only the laser dot moves in the captured image when the tool moves from S' to S . In Fig. 7(b), the laser dot I_1 is the one when the object surface is at the minimum allowed distance to the nozzle, and I_2 is when the object surface is at the maximum allowed distance to the nozzle.

As shown in Fig. 8, the correlation between the acceptance range of the laser dot positions in the captured images and the acceptance range of the gap distance can be established. For a given curvature of an object surface, the positions of I_1 and I_2 are known. Accordingly, their pixel positions in the captured images can be identified, which correspond to the minimum and maximum allowed gap distances, respectively. A fast image recognition algorithm and an automated error compensation method can thus be developed based on the pixel positions of the laser dot in the captured images. The tool tip will then move from S' toward S until the desired deposition gap is achieved.

3.4 Workspace Evaluation. For a 6-axis motion system based on the Stewart mechanism, not every position in the building space can be accessed. The workspace is constrained by two design variables: strut length and joint angle. Each strut must be within the range bounded by the maximum and minimum rod

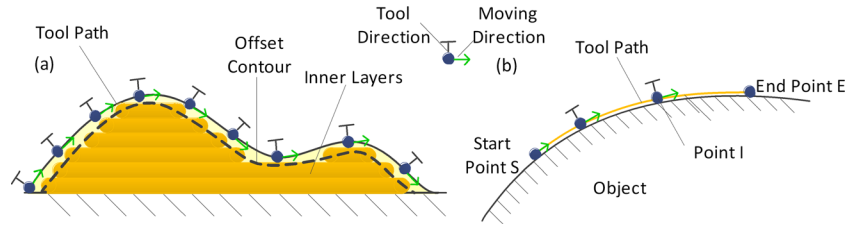
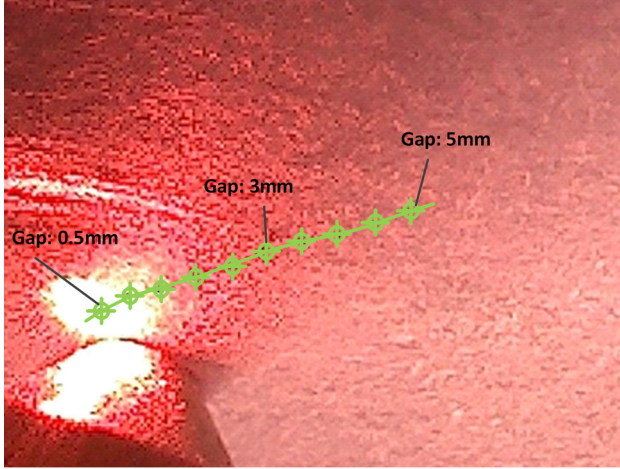
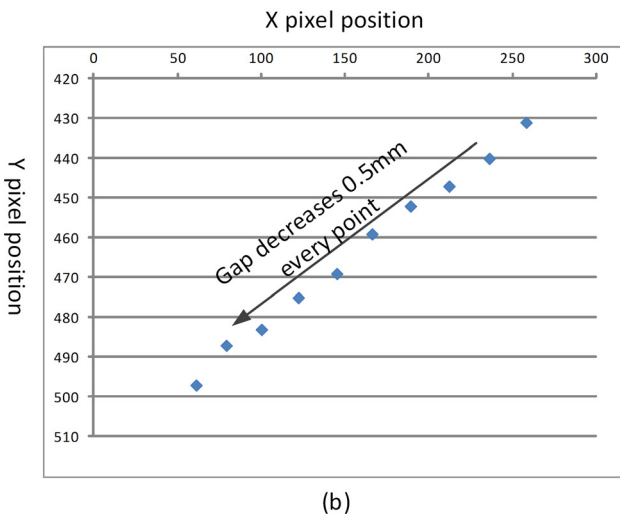


Fig. 6 Tool path planning for curve surface and build-around-inserts



(a)



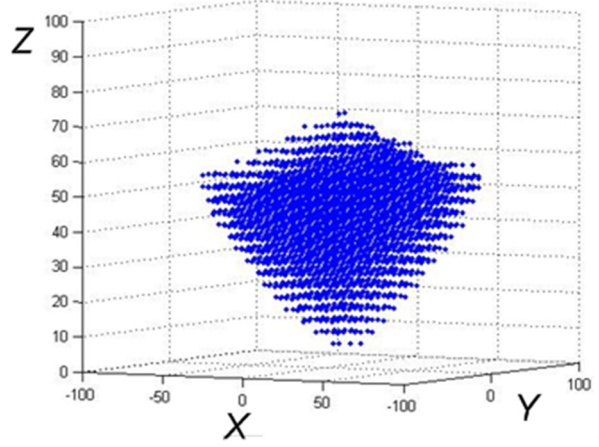
(b)

Fig. 8 Different gap distances versus pixel positions of the laser dot in the captured images

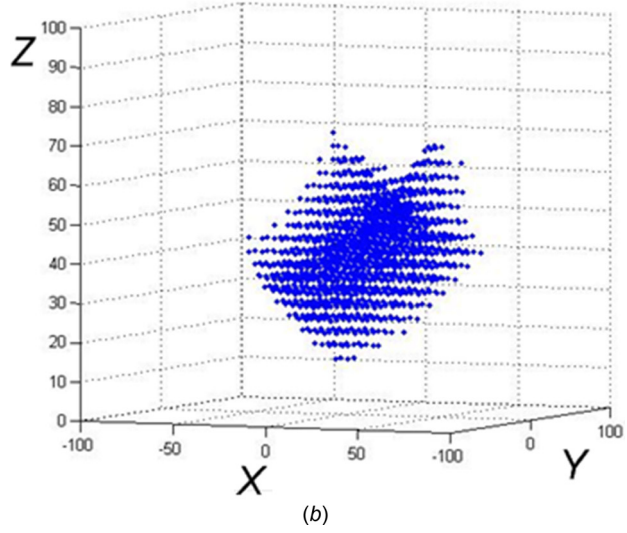
lengths. In our testbed, the working range of each strut is (170, 240) (mm). Both the base joint and platform joint have limited rotation angles as well. They significantly influence the effective working volume at a specific orientation of the tool. The constraint ranges of the base and platform joints in our machine are (-30 deg, 45 deg) and (60 deg, 120 deg), respectively. Accordingly, a library of the effective workspaces for different tool orientations can be generated. Figure 9 shows the workspace of our setup at two different tool orientations.

3.5 Movement Simulation and Control. A simulation software system is developed for computing the tool path based on Eqs. (1)-(5). Figure 10(a) shows the graphical user interface (GUI) of the developed simulation software system using Microsoft Visual C++. A G-code file with defined quaternion at each point can be opened in the viewing area. The position of each joint can be set in the left panel. The parameters are set based on the machine calibration, which will be discussed in Sec. 4. Before the simulation, an axis motion command file is generated from the G-code file to define the displacement of each strut based on Eqs. (3) and (4). The simulation starts only after the axis motion command file passes the constraint check. After that, the original G-code file with quaternion will be sent to the motion control software system.

Figure 10(b) shows the GUI of the developed motion control software system. The system is also developed using Microsoft Visual C++. Based on the axis motion commands generated by



(a)



(b)

Fig. 9 Workspaces at different tool orientations: (a) workspace when rotation angle is 0 deg and (b) workspace when rotating 10 deg around the X axis

the simulation system, the six linear motors will be controlled with the defined moving positions and speeds.

4 Platform Calibration

A set of 42 parameters including $\overrightarrow{OB_i}$, $\overrightarrow{OP_i}$, and l_{ij} ($i=1-6$) need to be set in the coordinate transformation models as described in Eqs. (3) and (4). The calibration of these parameter values is necessary for more accurate control of the 6-axis motion. The calibration approach that is used in our system is to iteratively update the system parameters by an error model such that a defined cost function can be minimized based on the given orientation and translation of the moving platform. A cost function for the 6-axis platform calibration is defined in Ref. [22]. It uses strut length measurement residual at all measured poses as the objective function. And the calibration problem can be formulated as a nonlinear optimization problem, which is given as follows:

$$\text{Minimize: } C = \sum_{j=1}^n \sum_{i=1}^6 s_{ij}$$

$$s_{ij} = (l_{ij} + \Delta l_{ij})^2 + \text{dev}^2 - (\overrightarrow{OB_i} - \overrightarrow{OB_j} - \mathbf{R} \cdot \overrightarrow{OP_i})^T$$

$$(\overrightarrow{OB_i} - \overrightarrow{OB_j} - \mathbf{R} \cdot \overrightarrow{OP_i}) \quad i = 1, 2, \dots, 6; j = 1, 2, \dots, n \quad (6)$$

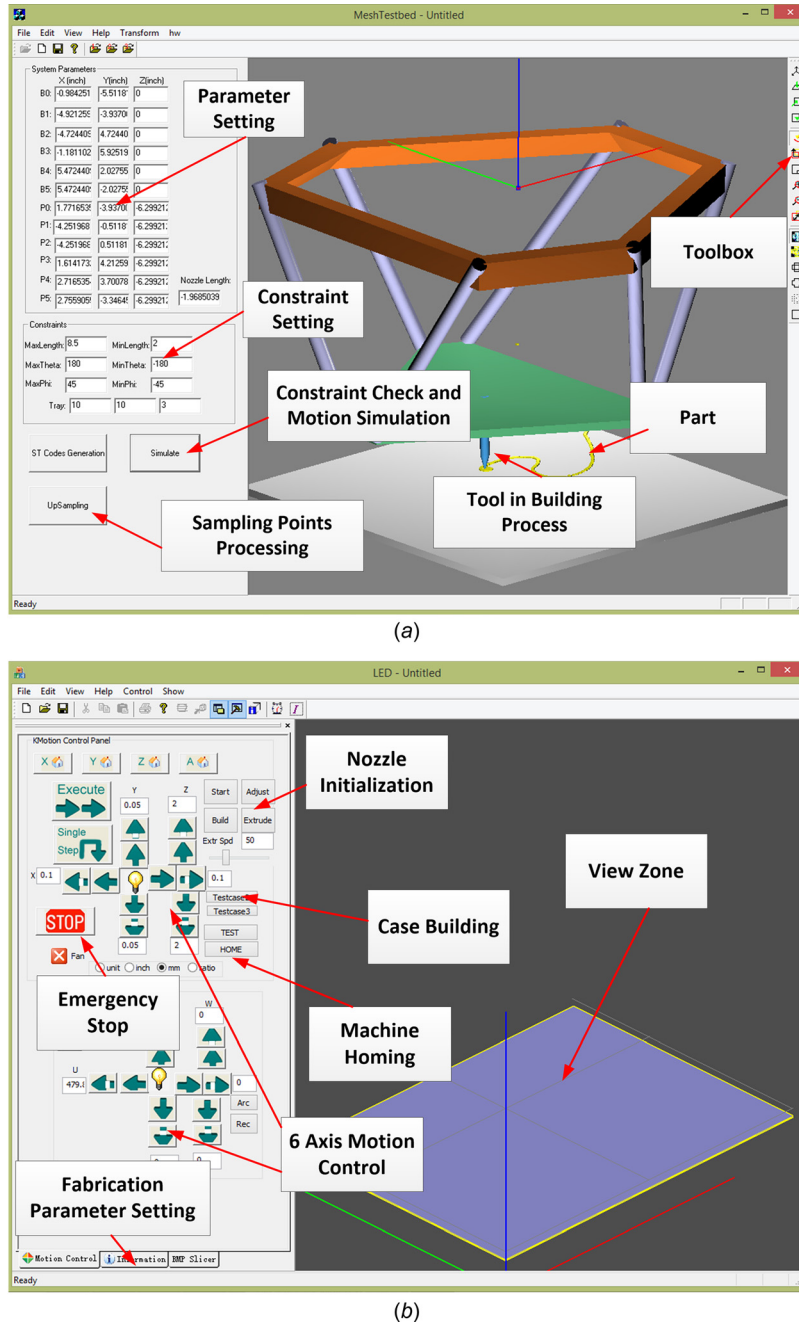


Fig. 10 Software systems developed for the parallel kinematic machine. (a) The simulation software system and (b) the motion control software system.

where n is the number of calibrated poses, and Δl_{ij} is the input moving displacement of the i th linear actuator at the j th calibrated pose of the platform.

From the kinematic equations (3) and (4), an error model can be generated in the form

$$s_{ij} = \mathbf{J} \cdot \Delta \rho \quad (7)$$

where J is the Jacobian matrix, $\Delta \rho = [\overrightarrow{d\mathbf{O}_B \mathbf{O}_P}, \overrightarrow{d\mathbf{O}_P \mathbf{P}_i}]^T$.

With the cost function and the error model, the nonlinear optimization function can be solved by the Gauss–Newton Algorithm.

No less than seven platform poses need to be collected in order to calibrate the machine using Eq. (6). In our experiments, a computer vision based method (refer to Fig. 11) is used in measuring the tool tip position and orientation. Two cameras are positioned orthogonal to each other. Three targets were placed on the moving

platform. Target 1 is located at the tool tip. Targets 2 and 3 were symmetric about the X axis of the moving frame. Each camera is calibrated such that the 3D point positions of the targets can be computed based on the captured 2D images of both cameras. This measurement approach was also used in Ref. [23]. Accordingly, the rotation matrix of the moving frame can be derived by the SVD (Singular Value Decomposition) method based on the positions of the three targets. More details on the camera calibration and 3D coordinate computation are given in Appendix B.

5 Multidirectional AM Process Overview

Based on the developed parallel kinematic machine, the major steps of a multidirectional AM system include: (1) tool path generation, (2) system coordinate transformation, (3) platform

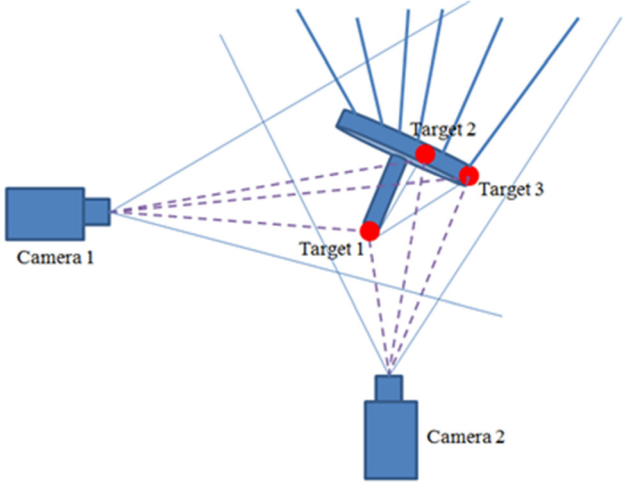


Fig. 11 An illustration of the platform pose measurement using two cameras

constraint checking, (4) movement simulation, and (5) part fabrication. In the tool path generation, an input CAD model is sliced in desired building orientation. The slicing direction can be determined based on surface normal or feature skeleton. A sliced layer contour can be sampled into a set of discrete points. Each sampling point can be used to compute the positions of the six linear actuators. At each point, the tool position and orientation are given. As discussed in Sec. 3, the 3D coordinate of the accumulative tool along with its accumulation orientation is converted into a transformation model to compute the related distances L_0-L_5 for the six struts of the machine. The displacement vector can then be sent to the motion controller to achieve the desired platform pose.

Note that not all the vectors computed based on the transformation process can be achieved by the prototype system. Several constraints exist including the limitation of actuators' stroke (i.e., (L_{\min}, L_{\max})), the limitation of the range of the passive joint, and the minimum distance between each actuator's lead screw. Hence, the computed results need to be checked using the known constraints. The tool path can be simulated in our software system to verify whether the six-dimensional motion vectors satisfy all the constraint equations. Finally, the verified six dimension coordinate vectors ($L_0, L_1, L_2, L_3, L_4, L_5$) can be sent to the control system to start the building process.

Figure 12 shows the data processing pipeline of the developed multidirectional AM system. A CNC control software system (e.g., Mach 3) may be used in converting a given CAD model into numeric control G-codes. However, the generated G-codes have only the coordinate positions along which the tool tip will travel. The tool can be positioned at various orientations for a given position in the G-code. As mentioned before, one good candidate is to align the tool orientation with the related surface normal of the object. Algorithms for computing appropriate tool orientations based on multidirectional material deposition requirements need to be studied for 6-axis AM systems in the future.

6 Experimental Tests

The developed parallel kinematic machine can be used with various multidirectional AM processes such as the FDM process and the CNC accumulation process [18]. A photo of the developed prototype with a filament extruder of the FDM process is shown in Fig. 13. In this section, some of the performed test cases are presented to demonstrate the capability of multidirectional FDM processes. A discussion of the challenges and future developments on multi-axis AM systems is also presented. A youtube video of the developed prototype system and some related experimental tests can be found at the link of Ref. [24].

6.1 Tests of Various Geometries. Different types of geometries are built using the developed 6-axis 3D printer to demonstrate its capability and verify some potential applications such as improving surface finishing.

- 3D curves

The multi-axis FDM system enables the tool to move freely in the space. Hence, similar to 3Doodler (a handheld 3D-printing pen at kickstarter), it can be used as a 3D printing pen to accurately draw in the air. Figure 14 shows a test case of a spiral curve. Note the extruding orientation is constantly changed for the given curve. The built 3D curve is also shown in Fig. 14. The shape is not a perfect spiral because the filament is still soft after being extruded out and slightly falls down until it gets hardened in the air.

- 3D surfaces

Figure 15(a) shows the CAD model of a designed test case on 3D surfaces to be fabricated by the multidirectional 3D printer. The planned tool paths are shown in Fig. 15(b). Note that the surface normal of the shape changes from the vertical direction n_1 to

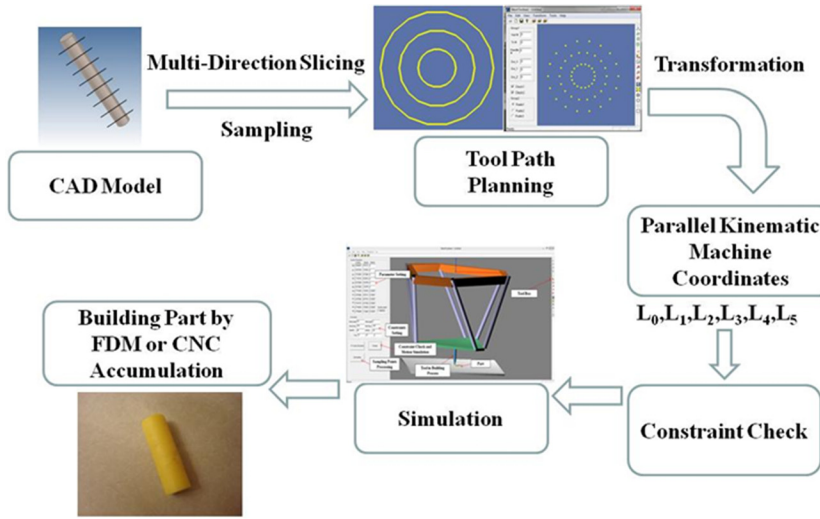


Fig. 12 Data processing pipeline of the multidirectional AM system using the parallel kinematic machine

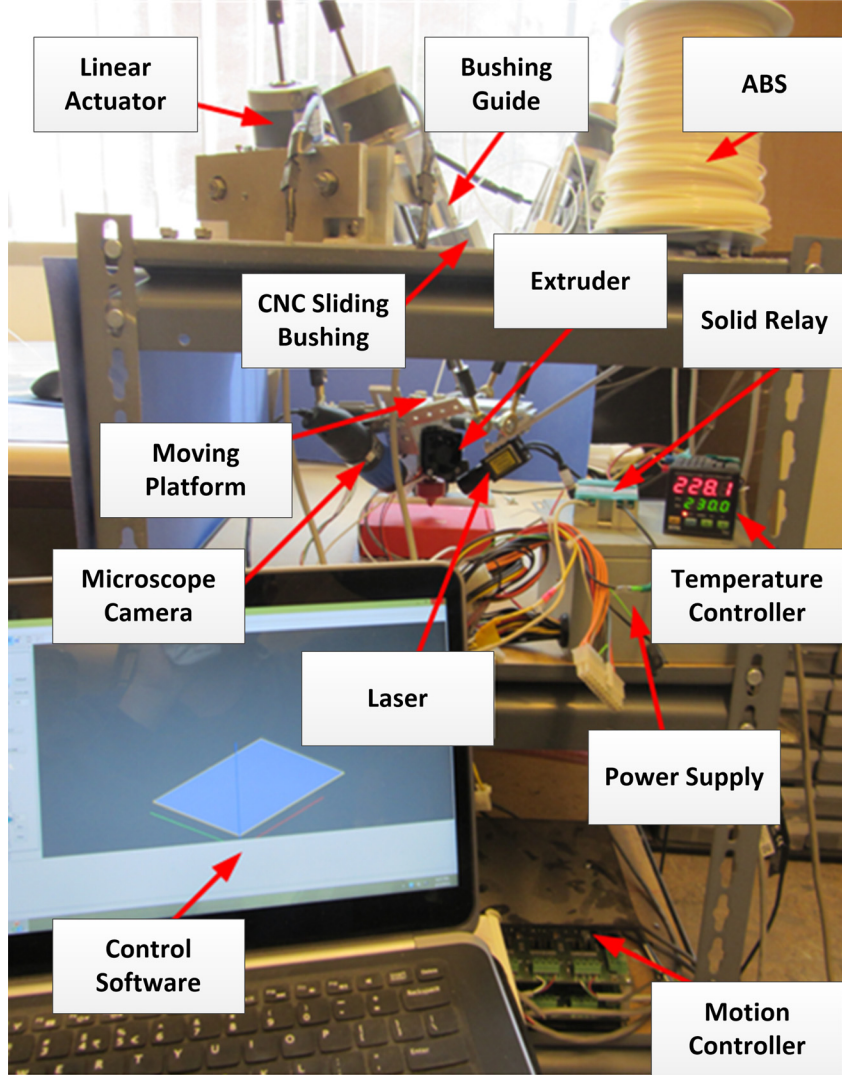


Fig. 13 The prototype system for the multidirectional FDM process

n_2 . For the horizontal portion of the model, n_1 (the Z axis) is chosen as the building direction. The fabrication of this portion is similar to the traditional linear-motion-based 3D printers. However, for the slope portion of the model, n_3 is chosen as the building direction for better attachment to the previously deposited layers. In comparison, if n_1 is still used for the surface, each deposited layer will not well attached to the previous layers since the compression force added by the nozzle will not aligned with n_3 .

Figure 16 shows the building results by using the multidirectional FDM system. The melted filament can attach well to the former solidified layers. Hence, the slope portion can be built without any supports by using the material deposition direction of n_3 instead of n_1 (i.e., the Z axis). Although without systematical study, we believe multidirectional FDM systems can enable less supports to be used for a given CAD model than the traditional layer-based FDM systems. It is especially important for some applications that require less or no supports during the building process.

- 3D parts with improved surface finish

Figure 17 shows a test case to verify whether the multidirectional FDM system can improve the surface quality of a curved surface. The model of a curved surface is shown in Fig. 17(a). Conventionally, this model is built by depositing multiple 2D layers along the Z axis. Accordingly, the related tool path is shown in Fig. 17(a) as planar contours. However, this yields a

rough surface finish with very obvious staircase effect especially for near-vertical surfaces (refer to the built model in Fig. 17(b) and the dashed lines in Fig. 17(c)). As discussed in Sec. 3.2, curved tool path based on the newly developed 6-axis deposition capability can make the contour consistent with the original design without the staircase effect. The planned curved tool path is shown in Fig. 17(a) as the lines on the surface. The accordingly built model is shown in Fig. 17(b) and a magnified view of the curved surface is shown in Fig. 17(d).

6.2 Building-Around-Inserts. Each manufacturing process has its unique properties. For example, the injection molding process is fast and low-cost; however, the complexity of fabricated shapes is limited. In comparison, the AM processes can fabricate very complex shapes; however, the fabrication speed is relatively slow. Hence, it is desired to have an AM process that can incorporate existing components that are fabricated by other manufacturing processes (e.g., injection molding) in its building process. Such capability, if fully realized, would enable hybrid manufacturing processes by taking advantage of different fabrication processes. Consequently, a product component may have complex shape, heterogeneous material properties, and multifunctionality with embedded sensors, actuators, optics, etc.

- Building features on slanted flat planes

In the first test case of building-around-inserts, three characters “USC” are to be built on a slanted plane of a box (refer to Fig.

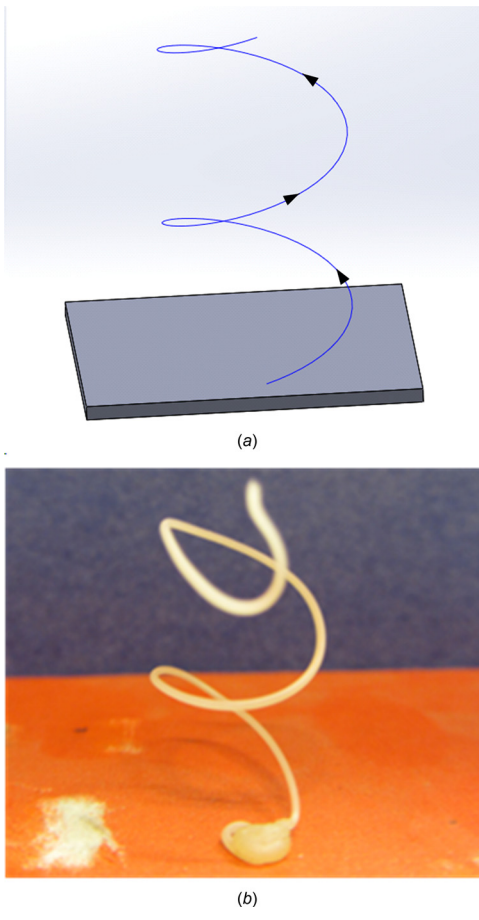


Fig. 14 A 3D spiral curve drawn by the multi-axis FDM system

18(a)). In the linear-motion-based FDM machines, a nozzle can only extrude filaments vertically. Hence, it would be difficult to build features on such a surface since a large gap will exist between the slanted plane and the vertical nozzle in order to avoid the collision between them. In comparison, a desired gap distance can be achieved by rotating the nozzle to be perpendicular to the plane. Accordingly, the characters can be fabricated on the slanted plane, which are shown in Fig. 18(b).

- Building features on freeform surfaces

In another test case of building-around-inserts, a curved line needs to be deposited on the surface of a bottle that is made by another manufacturing process. This demonstrates the capability of multi-axis AM process on building arbitrary shapes on an existing object. As shown in Fig. 19, the bottle body is a cylinder with a diameter of ~ 31 mm. In order to build a curved line along its surface, the nozzle direction needs to be constantly changed in order to keep the tool with a building direction that is coaxial with the surface normal. The nozzle orientations at the start and end positions are shown Fig. 19(a). The angles of the nozzle will change from -20 deg to $+20$ deg during the building process. Figure 19(b) shows the fabricated result. By this method, we could freely add new features to an existing object or repair any portion that has been broken. In our previous work [23], a 3D scanner was integrated in a CNC accumulation system such that an inserted object can be scanned and the related tool path can be automatically generated based on the 3D scanning results.

6.3 Discussion. The purpose of the work is to investigate the construction of a low-cost multidirectional AM system and to demonstrate the unique benefits and challenges of multidirectional AM systems. The Stewart mechanism and the process planning for the parallel kinematic based AM machine are presented. To

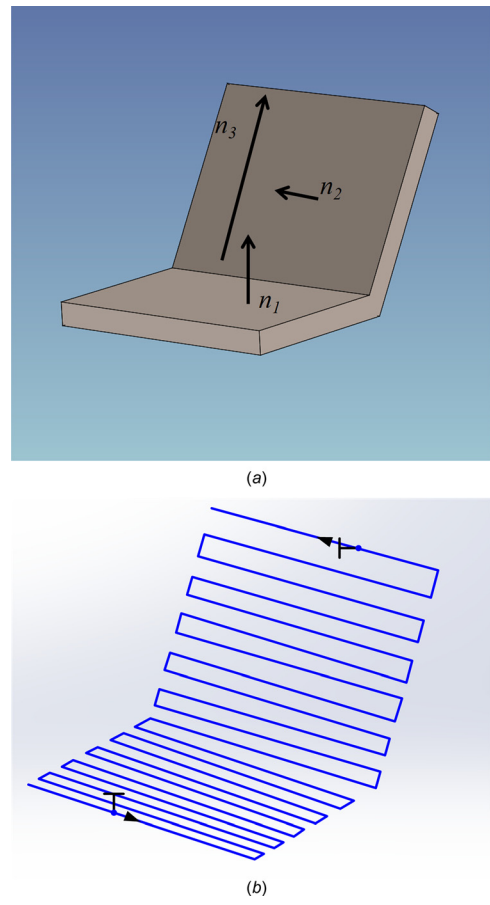
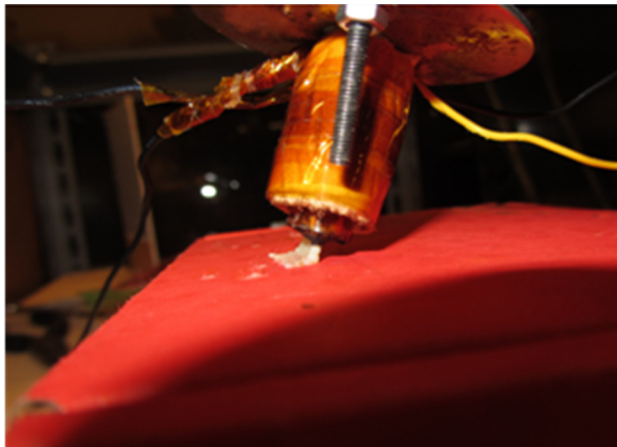


Fig. 15 A model with a slanted surface to be built. (a) Different surface normals and related building directions and (b) planned tool path for the 3D surfaces.

demonstrate the feasibility, a simple design of an extrusion nozzle is used with ABS filament as the raw material. The achieved design serves as a rapid prototyping example of a successful low-cost and fully operational multidirectional AM system for future researchers and developers. The specifications of our multidirectional AM machine are given as follows.

- (1) Working volume. The working volume of our system is designed as $100\text{ mm} \times 100\text{ mm} \times 100\text{ mm}$. The working volume based on the Stewart mechanism depends on the travel range of the lead screws and slide bushings, as well as the angle range of the ball joints.
- (2) Rotation angle of the platform. The rotation angle of the moving frame in our prototype system is ± 30 deg. Like the working volume, the rotation range mainly depends on the selected ball joints, and the travel ranges of lead screws and slide bushings.
- (3) Accuracy. The accuracy of the prototype system is < 0.5 mm. The larger the tool angle is, the lower the accuracy will be. It is mainly due to the errors in the universal and ball joints. However, using the laser-camera feedback control method (refer to Sec. 3.3), the deposition gap can achieve a much smaller value (0.1 mm–0.2 mm).

The constructed prototype system was intentionally built out of low-cost components in order to verify the feasibility of multidirectional 3D printers in desired price range. There are various improvements that can be incorporated in the system, e.g., a better extrusion nozzle and a more compact frame design. In addition, the speed, precision, and orientation capacity of system can all be

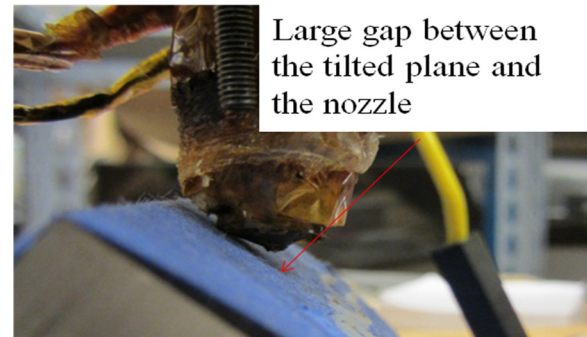


(a)

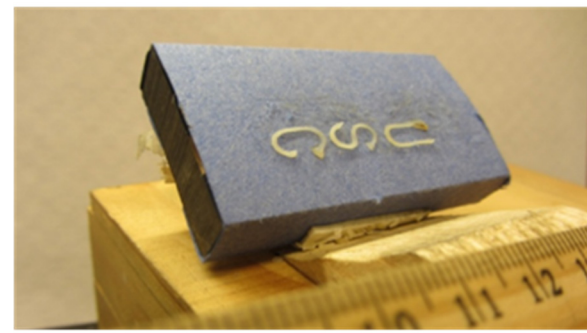


(b)

Fig. 16 Test results. (a) Part fabrication by the FDM extrusion in a tilted angle and (b) built part.



(a)



(b)

Fig. 18 Test results of building-around-inserts. (a) Problem with the vertical building on a slanted plane and (b) built characters on the plane.

improved by replacing the components with more expensive and precise ones.

The work successfully demonstrates the adoption of the Stewart mechanism in an AM process—FDM. The developed multidirectional FDM process has unique capability and brings many advantages. Recently, Pan et al. [25] presented a multidirectional AM process for conformal feature fabrication on curved surfaces. Denkena et al. [26] reviewed how multidirectional fabrication can be used in conventional machining processes. However, there are still tremendous research challenges to be addressed in order to fully utilize the advantages of multidirectional AM processes. We believe some of such research opportunities for future AM process development include:

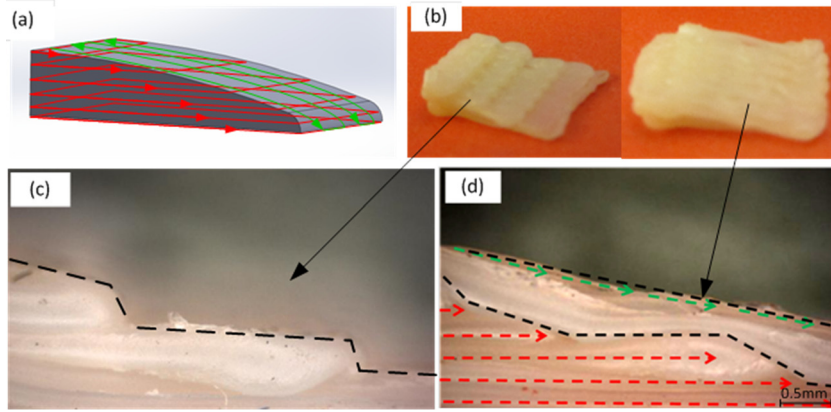


Fig. 17 Test results of 3D parts with improved surface finish. (a) A curved surface and planned tool paths; (b) built parts using two different approaches; (c) a magnified surface fabricated by the unidirectional AM approach; and (d) a magnified surface fabricated by the multidirectional AM approach.

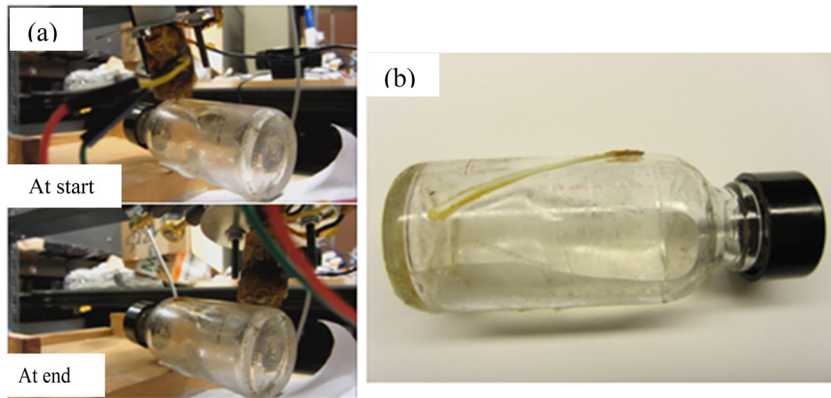


Fig. 19 Test results of building-around-inserts. (a) FDM nozzle at different positions and (b) built result on the curved surface.

- (1) Physical modeling with respect to material deposition directions. Material deposition orientations directly determine the surface finish, stress distribution, required supports, and material properties in the fabricated parts. It is desired to explore the relations between and each of these properties and material deposition directions. These design requirements should be given along with the CAD model. Currently, the boundary representation (B-rep) based CAD models for representing shapes are not sufficient in conveying all the fabrication information and may need to be extended.
- (2) Multidirectional process planning algorithm. One significant benefit of the layer-based AM processes is the process planning algorithm is significantly simplified by using a single building direction and uniform layers. In comparison, the multidirectional AM processes, by significantly increase the allowable motions between the tool and the work piece, may address issues such as staircase effect and inconsistent material properties. However, the increased design freedom will also require more sophisticated process planning algorithms to be developed. We believe the AM community can learn from the multi-axis CNC machining process on such algorithm development.
- (3) Intelligent machine design. The hardware construction of a multidirectional AM system will be more complex than a unidirectional AM system. To achieve desired fabrication performance, the machine development of a multidirectional AM system needs to consider condition monitoring, product quality control, and/or real-time fault diagnosis. For example, some process monitoring and control techniques can be considered including a dynamic position feedback of the accumulation tool, a force feedback sensor during the material extruding process, an iterative kinematics solving strategy, and a real-time orientation adjustment mechanism. Such smart sensors and controllers that are integrated in the multidirectional AM systems can also benefit the traditional layer-based AM systems.

7 Conclusion and Future Work

In the paper, a low-cost 6-axis AM system based on the Stewart mechanism has been developed for multidirectional deposition processes. Our design is modular and can easily be incorporated with various accumulation tools. The system based on the six linear actuators is relatively inexpensive. It can move tools in a satisfactory speed. In addition, an integrated laser-camera system can correct backlash errors at the initial positions such that an accurate deposition gap is ensured to eliminate the risk of collision. By

enabling full 6-axis motions between an accumulative tool and a workpiece, the multidirectional AM system can deposit materials from desired directions. Multiple test cases have been performed to demonstrate the multidirectional AM processes can overcome the drawbacks of the traditional layer-based AM processes including dense supports, staircase effect, and the limitations on building-around-inserts.

The multidirectional AM processes open the door for more intelligent tool path planning beyond the layer-based approach that is dominant in current AM processes. One of such possibilities is demonstrated in our paper (refer to Figs. 6 and 17). However, a significant amount of work is still required on developing automatic tool path planning methods and algorithms in the future. In addition, the integration of real-time sensors and the use of close loop control methods are critical for future AM process development. We plan to further develop the presented laser-camera system and also investigate other real-time sensors in improving the building quality of the layer-based and multidirectional AM processes.

Acknowledgment

We acknowledge the help of Tom Kerekes from Dynomotion Inc. for sharing his 3-axis parallel kinematic machine design and the use of Kflop control board. We also acknowledge the support of the NSF Grant No. CMMI-1151191.

Appendix A

Hardware Components of Prototype System

Table 1 Cost of the prototype system

Item	Quantity	Price each
Linear actuator	6	\$75
Aluminum plate	4 in. × 4 in., 12 in. × 24 in.	\$78
Aluminum angle	4'	\$32
Bearing	24	\$7.0
Lead screw	6	\$10
3 in. alloy steel thread stud	12	\$1.5
Ball joint	6	\$7.0
Aluminum rod	6'	\$10
Others (screws, nuts, slides, bushing, etc.)	NA	\$80
Motor controller	1	\$500
Total	NA	\$1438

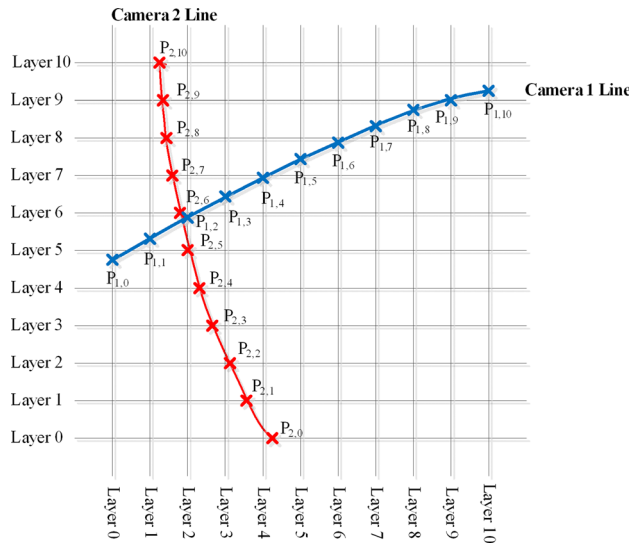


Fig. 20 Point retrieval by calculating the closing point between two camera lines

Appendix B

Measurement of Platform Poses

Since 42 system parameters are unknown in the axis displacement generation model, the measurement of seven or more poses are required since each pose has six variables. In our experiments, twelve poses are randomly chosen, twice the minimum pose number, to ensure the accuracy of the calibrated parameter values.

B.1 Camera Calibration. The two cameras are first calibrated in order to identify the relation between a pixel on a 2D image and its corresponding 3D position. Considering the nonlinearity of a camera, the working volume is equally divided into 11 layers along the X and Y axes for camera 1 and 2, respectively. The distance between two neighboring layers is 5 mm. A printed chessboard is placed at each layer; an image will be taken to analyze all the corner points of the chessboard. Since the coordinates of each corner point on the chessboard are known, a database of the relations between an image pixel and its base frame coordinate at each layer can be established. For example, suppose the i th corner point on the chessboard at layer j in camera 1's calibration volume has world coordinate $(x_{ij}^1, y_{ij}^1, z_{ij}^1)$. After its pixel (x_{image}, y_{image}) in the image is identified, a database for camera 1 can be obtained in the form of $(x_{ij}^1, y_{ij}^1, z_{ij}^1, x_{image}, y_{image})$. Inversely, if pixel position of a point on the image is given as (x_{image}, y_{image}) , its corresponding 3D position at layer j can be calculated through the bilinear interpolation of the four corners of the checker box in which the pixel falls.

B.2 3D Point Coordinate Computation. For a certain platform pose, the three targets on the moving platform can be captured by the two cameras (refer to Fig. 20). Accordingly, two groups of pixel positions $(x_{image}^1, y_{image}^1)$ and $(x_{image}^2, y_{image}^2)$ from cameras 1 and 2 can be recorded for any target. Since the depth of the target in the camera's view volume is unknown, we can calculate its 3D position at each layer first. For example, the world coordinates $P_{1,0}$ can be retrieved from the database related to pixel $(x_{image}^1, y_{image}^1)$ at layer 0. Similarly all these 3D coordinates identified at each layer will form a distorted camera view line (refer to Fig. 20). For the same target, the two camera lines may not exactly intersect due to the camera calibration errors. Instead, the

3D coordinate of the target can be computed as the point with the minimum distances to both camera lines. For example, the closest distance between the two camera lines as shown in Fig. 20 is between segment $P_{1,1}P_{1,2}$ and segment $P_{2,5}P_{2,6}$.

References

- [1] Sager, B., 2006, "Stereolithography Characterization for Surface Finish Improvement: Inverse Design Methods for Process Planning," Ph.D. thesis, Georgia Institute of Technology, Atlanta, GA.
- [2] Sager, B., and Rosen, D. W., 2008, "Use of Parameter Estimation for Stereolithography Surface Finish Improvement," *Rapid Prototyping J.*, **14**(4), pp. 213–220.
- [3] Pandey, P. M., Reddy, N. V., and Dhande, S. G., 2003, "Improvement of Surface Finish by Staircase Machining in Fused Deposition Modeling," *J. Mater. Process. Technol.*, **132**(1), pp. 323–331.
- [4] Mason, A., 2006, "Multi-Axis Hybrid Rapid Prototyping Using Fusion Deposition Modeling," Master thesis, Ryerson University, Toronto, Ontario, Canada.
- [5] Narahara, H., and Saito, K., 1995, "Study on the Improvement of Surface Roughness of Complex Model Created by Three Dimensional Photofabrication—Proposal of Lift Up Irradiation Method," *J. Jpn. Soc. Precis. Eng.*, **61**(2), pp. 233–237.
- [6] Pan, Y., Zhao, X., Zhou, C., and Chen, Y., 2012, "Smooth Surface Fabrication in the Mask Projection Based Stereolithography," *SME J. Manuf. Processes*, **14**(4), pp. 460–470.
- [7] Kataria, A., and Rosen, D. W., 2001, "Building Around Inserts: Methods for Fabricating Complex Devices in Stereolithography," *Rapid Prototyping J.*, **7**(5), pp. 253–262.
- [8] Ruan, J., Eiamsa-ard, K., and Liou, F. W., 2005, "Automatic Process Planning and Toolpath Generation of a Multiaxis Hybrid Manufacturing System," *J. Manuf. Processes*, **7**(1), pp. 57–68.
- [9] Singh, P., Moon, Y., Dutta, D., and Kota, S., 2003, "Design of a Customized Multi-directional Layered Deposition System Based on Part Geometry," Annual Solid Freeform Fabrication Symposium, Austin, TX, Aug. 4–6.
- [10] McLean, M. A., Shannon, G. J., and Steen, W. M., 1997, "Laser Generating Metallic Components," International Symposium on Gas Flow and Chemical Lasers and High-Power Laser Conference, Edinburgh, UK, Apr. 4.
- [11] Kim, J., 2011, "Advanced Multi-Directional UV Lithography for Three Dimensional (3D) Micro/Nano Structures," Ph.D. thesis, State University of New York at Buffalo, Buffalo, NY.
- [12] Pinkerton, A. J., Wang, W., and Li, L., 2008, "Component Repair Using Laser Direct Metal Deposition," *J. Eng. Manuf.*, **222**(7), pp. 827–836.
- [13] Dutta, B., Palaniswamy, S., Choi, J., Song, L. J., and Mazumder, J., 2011, "Additive Manufacturing by Direct Metal Deposition," *Adv. Mater. Processes*, **169**(5), pp. 33–36.
- [14] Choi, J., and Chang, Y., 2006, "Analysis of Laser Control Effects for Direct Metal Deposition Process," *J. Mech. Sci. Technol.*, **20**(10), pp. 1680–1690.
- [15] Dutta, B., Singh, V., Natu, H., and Choi, J., 2009, "Direct Metal Deposition: Six-axis Direct Metal Deposition Technology Enables Creation/Coating of New Parts or Remanufacturing of Damaged Parts With Near Net-shape," *Adv. Mater. Processes*, **167**(3), pp. 29–31.
- [16] Ruan, J., Tang, L., Liou, F. W., and Landers, R. G., 2010, "Direct Three-Dimensional Layer Metal Deposition," *ASME J. Manuf. Sci. Eng.*, **132**(6), p. 064502.
- [17] Milewski, J. O., Lewis, G. K., Thoma, D. J., Keel, G. I., Nemec, R. B., and Reinert, R. A., 1988, "Directed Light Fabrication of A Solid Metal Hemisphere Using 5-Axis Powder Deposition," *J. Mater. Process. Technol.*, **75**(1–3), pp. 165–172.
- [18] Chen, Y., Zhou, C., and Lao, J., 2011, "A Layerless Additive Manufacturing Process Based on CNC Accumulation," *Rapid Prototyping J.*, **17**(3), pp. 218–227.
- [19] Saputra, V. B., Ng, C. C., Ong, S. K., and Nee, A. Y. C., 2009, "Development and Trajectory Planning of a Hybrid Serial-Parallel Manipulator," *Asian Int. J. Sci. Technol. Proj. Manuf. Eng.*, **2**(1), pp. 99–115.
- [20] Ng, C. C., Ong, S. K., and Nee, A. Y. C., 2006, "Design and Development of 3-DOF Modular Micro Parallel Kinematic Manipulator," *Int. J. Adv. Manuf. Technol.*, **31**(1–2), pp. 188–200.
- [21] Chen, Y., and Wang, C. C. L., 2011, "Uniform Offsetting of Polygonal Model Based on Layered Depth-Normal Images," *Comput.-Aided Des.*, **43**(1), pp. 31–46.
- [22] Zhuang, H., Yan, J., and Masory, O., 1998, "Calibration of Stewart Platforms and Other Parallel Manipulators by Minimizing Inverse Kinematic Residuals," *J. Rob. Syst.*, **15**(7), pp. 395–405.
- [23] Zhao, X., Pan, Y., Zhou, C., Chen, Y., and Wang, C. C. L., 2013, "An Integrated CNC Accumulation System for Automatic Building-around-inserts," *SME J. Manuf. Processes*, **15**(4), pp. 432–443.
- [24] Song, X., Pan, Y., and Chen, Y., Last Accessed Sept. 22, 2013, <http://www.youtube.com/watch?v=qGyiXFGvkqe>
- [25] Pan, Y., Zhou, C., Chen, Y., and Partanen, J., 2014, "Multitool and Multi-Axis Computer Numerically Controlled Accumulation for Fabricating Conformal Features on Curved Surfaces," *ASME J. Manuf. Sci. Eng.*, **136**(3), p. 031007.
- [26] Denkena, B., Turger, A., Behrens, L., and Krawczyk, T., 2012, "Five-Axis Grinding With Toric Tools: A Status Review," *ASME J. Manuf. Sci. Eng.*, **134**(5), p. 054001.